RSC Advances

ROYAL SOCIETY OF CHEMISTRY

www.rsc.org/advances

Preparation and characterization of highly sodium ion conducting Na_3PS_4-Na_4SiS_4 solid electrolytes

Naoto Tanibata, Kousuke Noi, Akitoshi Hayashi, Masahiro Tatsumisago

Department of Applied Chemistry, Graduate School of Engineering,

Osaka Prefecture University, 1-1, Gakuen-cho, Naka-ku, Sakai, Osaka, 599-8531, Japan.

Corresponding author:

Akitoshi Hayashi (Associate Professor)

Department of Applied Chemistry, Graduate School of Engineering,

Osaka Prefecture University,

1-1 Gakuen-cho, Naka-ku, Sakai, Osaka 599-8531, JAPAN

Tel.: +81-72-2549331; Fax.: +81-72-2549334

E-mail address: hayashi@chem.osakafu-u.ac.jp.

Abstract

This study investigated electrical and electrochemical properties of $(100\text{-}x)Na_3PS_4 \cdot xNa_4SiS_4$ (mol%) glass–ceramics prepared using mechanical milling and consecutive heat treatment. Glass–ceramics at the compositions of $0 \leq x \leq 10$ exhibited higher conductivity than 10^{-4} S cm^{-1} at room temperature, which was achieved by precipitation of cubic Na_3PS_4 crystal with high sodium ion conductivity. The conductivity increased concomitantly with increasing Na_4SiS_4 contents at compositions of $0 \leq x \leq 6$. The glass–ceramic with 6 mol% Na_4SiS_4 exhibited conductivity of 7.4×10^{-4} S cm^{-1} at room temperature, which is the highest value reported for Na^+ ion conducting sulfides to date. The conductivities of the glass–ceramics in the composition range of $25 \leq x \leq 100$, where unknown phases are crystallized, were 10^{-7} – 10^{-5} S cm^{-1}. These were lower than the conductivities of the corresponding glasses before heat treatment. The $90Na_3PS_4 \cdot 10Na_4SiS_4$ electrolyte showed a wide electrochemical window of 5 V.

1. Introduction

Rechargeable batteries capable of storing renewable energy generated from solar and wind power sources are a key technology in the effort to reduce greenhouse gas emissions. Rechargeable lithium batteries are widely used today in portable power storage applications. However, flammable organic liquid electrolytes present safety concerns. Moreover, lithium resources are limited and are present in remote or in politically sensitive areas. Increasing demand for large lithium-ion batteries in electric vehicles will engender rising costs of lithium resources. Further development of safe, low-cost lithium batteries is necessary for widespread popularization of large rechargeable batteries for use in vehicles and distributed power applications. All-solid-state batteries are safe because they do not suffer from leakage, volatilization, or flammability of electrolytes. They employ inorganic solid electrolytes instead of organic liquid electrolytes.[1–2] Rechargeable sodium-ion batteries are more suitable than lithium-ion batteries for use in energy storage systems from the viewpoint of production costs based on abundant sodium sources.[3–6] Therefore, all-solid-state sodium secondary batteries are anticipated for use as next-generation batteries providing high safety and low cost for use with distributed energy sources.

Very recently, we reported that all-solid-state sodium batteries with a Na_3PS_4 glass–ceramic electrolyte operated successfully as rechargeable batteries at room temperature.[7] The high conductivity of the Na_3PS_4 glass–ceramic was 4.6×10^{-4} S cm^{-1} at room temperature,[8] which was achieved by precipitation of the cubic Na_3PS_4 crystal with high Na^+ ion conductivity. To improve all-solid-state sodium battery performance, solid electrolytes with higher Na^+ ion conductivity must be developed.

For lithium ion conductors, Kanno *et al*. reported that Li_3PS_4-based crystals, where Li_4GeS_4 was partially substituted for Li_3PS_4, showed higher conductivity than Li_3PS_4 and Li_4GeS_4 crystals.[9] Recently, $Li_{10}GeP_2S_{12}$ crystal showed extremely high lithium ion conductivity of more than 10^{-2} S cm^{-1} at room temperature.[10] We also reported that the partial substitution of Li_4SiS_4 for Li_3PS_4 was effective for increasing the conductivity of Li_3PS_4 glass–ceramics.[11] To increase the conductivity of Na_3PS_4

glass–ceramics, we have particularly studied partial substitution of Na_4SiS_4 for Na_3PS_4 because the introduction of Si element is effective for increasing conductivity of the Li_3PS_4 glass–ceramic system.

For this study, (100-x)Na_3PS_4•xNa_4SiS_4 (mol%) glass–ceramics were prepared using mechanical milling and heat treatment (HT). The relation between crystals precipitated in the (100-x)Na_3PS_4•xNa_4SiS_4 glass–ceramics and their ionic conductivities was investigated. Thermal and electrochemical properties of glass–ceramics were also evaluated.

2. Experimental

A mixture of Na_2S (> 99.1%; Nagao Co.), P_2S_5 (> 99%; Aldrich Chemical Co. Inc.), and SiS_2 (> 99.9%; Furuuchi Chemical Co.) powders at the composition of (100-x)Na_3PS_4•xNa_4SiS_4 (mol%) was mechanically milled at ambient temperature using a planetary ball mill apparatus (Pulverisette 7; Fritsch GmbH) with a zirconia pot (45 ml) and 500 zirconia balls (4 mm diameter). The rotation speed was 510 rpm. Milling durations were 1.5–25 hours. After mechanical milling, the powdered samples were compressed with a conventional uniaxial cold press to prepare 10-mm-diameter, 1–1.5-mm-thick pellets. To obtain the glass–ceramics, the milled sample pellets were crystallized by heating at an appropriate temperature between 220°C and 360°C in an electric furnace for 2 h. The heating temperature was selected based on crystallization temperatures determined using differential thermal analysis (DTA). All processes were performed in a dry Ar atmosphere. The XRD measurements of the prepared materials were performed using Cu Kα with a diffractometer (Ultima IV; Rigaku Corp.). Diffraction data were collected in 0.01° steps from 10.0° to 60.0° in 2θ. DTA was performed using a thermal analyzer (thermo Plus TG8110; Rigaku Corp.). The heating rate was 10°C min^{-1}.

Ionic conductivities of the pelletized (100-x)Na_3PS_4•xNa_4SiS_4 milled samples and the heated samples prepared at various temperatures were evaluated using AC impedance measurements. The pellets were then coated with carbon paste on both faces to form ion-blocking electrodes. Two stainless steel

disks coupled with Pt wires were attached to the pellets as current collectors. AC impedance measurements were conducted for the cell using dry Ar gas flow with an impedance analyzer (1260; Solartron Analytical) at frequencies of 10 Hz to 8 MHz. Cyclic voltammetry measurements were conducted to investigate the electrochemical properties of the solid electrolytes. A stainless-steel disk as the working electrode and a sodium foil as the counter and reference electrode were attached to each face of the pellet. Cyclic voltammograms of the $90Na_3PS_4 \bullet 10Na_4SiS_4$ glass–ceramic were obtained with a scan rate of 5 mV s^{-1} between −0.5 and 5.0 V (vs. Na^+/Na) at 25 °C. A stainless-steel disk as the working electrode and a sodium foil as the counter and reference electrode were attached to each pellet face.

3. Results and Discussion

Figure 1 presents XRD patterns of the $(100\text{-}x)Na_3PS_4 \bullet xNa_4SiS_4$ samples prepared using mechanical milling. A cubic Na_3PS_4 phase was crystallized using a milling process in the samples at the composition range of $0 \leq x \leq 10$. We recently reported the cubic Na_3PS_4 phase that was obtained directly at the composition x=0 using Na_2S (Nagao Co.) as a starting sodium source,[8] while a Na_3PS_4 glass was prepared using Na_2S (Aldrich Co.).[7] Halo patterns were observed for samples between $25 \leq x \leq 100$, suggesting that glass samples were obtained.

Figure 2 shows DTA curves of the $(100\text{-}x)Na_3PS_4 \bullet xNa_4SiS_4$ milled samples. An exothermic peak attributable to crystallization was observed for the glass samples (x = 67 and 100). A broad exothermic peak was also observed for the samples (x = 0 and 10) where the cubic Na_3PS_4 phase was precipitated directly using a milling process. A glassy component partially remaining in the milled samples was crystallized. The pelletized samples were thus heat treated at over those crystallization temperatures as shown in Figure 2. The heat-treated samples are described as “glass–ceramics”.

Figure 3 shows XRD patterns of the $(100\text{-}x)Na_3PS_4 \bullet xNa_4SiS_4$ glass–ceramics. Silicon was used as an internal standard in XRD measurements. In the composition range of $0 \leq x \leq 10$, the intensity of the

peaks attributable to the cubic Na_3PS_4 increased. No new peaks attributable to other crystalline phases appeared. The crystallite size of cubic Na_3PS_4 at the composition of x=0 was determined by the Scherrer equation from the full width of half maximum of the peak with the highest intensity; the size of cubic Na_3PS_4 increased from *ca.* 13 nm to *ca.* 22 nm by the heat treatment. At the composition of *x*=25, new peaks in addition to the peaks of the cubic Na_3PS_4 were observed. Only new peaks appeared at the composition of *x*=67. The pattern at the composition of *x*=100 differed completely from that of *x*=67, indicating that a different unknown phase was precipitated in the glass–ceramic of *x*=100. Unfortunately, we have not identified these two unknown phases at the present stage. In the following discussion, we describe the unknown phases observed at the composition of *x*=67 and *x*=100 as "unknown I" and "unknown II" phases, respectively.

The temperature dependence of conductivity of the $94Na_3PS_4 \bullet 6Na_4SiS_4$ glass–ceramic pellets is portrayed in Figure 4. The inset shows a complex impedance plot of the glass–ceramic measured at 25°C. In the plot, a part of a semicircle in the higher-frequency region and a spike in the lower-frequency region were observed, suggesting that the glass–ceramic behaves as a typical ionic conductor. The former component was attributed to bulk and grain boundary contributions, which were not separated distinctly. The total conductivity, which includes bulk and grain-boundary components, was determined from the total resistance (R_{total}) at the cross-section of the semicircle and the spike on the x-axis. The total conductivity obeys the Arrhenius equation, $\sigma = \sigma_0 \exp(-E_a / RT)$. Therefore, activation energy (E_a) for conduction was calculated from the slope in the temperature dependence of conductivity.

Figure 5(a) shows the composition dependence of ambient temperature conductivities of the $(100\text{-}x)Na_3PS_4 \bullet xNa_4SiS_4$ samples. Open circles denote the conductivity for the as-prepared samples by milling. In the composition range of $25 \leq x \leq 100$, where amorphous samples were obtained, the conductivities of the as-prepared samples were about 10^{-5} S cm^{-1}. In the composition range of $0 \leq x \leq 10$, where the samples included the cubic Na_3PS_4 phase, the conductivities were $10^{-5} - 10^{-4}$ S cm^{-1}. Closed

circles denote conductivity for the heat-treated samples (glass–ceramics). In the composition range of 25 ≤ x ≤ 100, where the unknown I or II phase was precipitated, the conductivities of the glass–ceramics were 10^{-7} – 10^{-5} S cm^{-1}; the conductivities were lower than those of as-prepared samples. Conductivities of the unknown I or II crystals are expected to be lower than those of the amorphous samples. In the composition range of 0 ≤ x ≤ 10, where the cubic Na_3PS_4 phase was mainly crystallized, the conductivities increased to more than 10^{-4} S cm^{-1} by heat treatment. All the glass–ceramics in the composition range were prepared by heat-treatment at 220°C. Figure 5(b) shows the composition dependence of ambient temperature conductivities and activation energies for conduction of the (100-x)Na_3PS_4•xNa_4SiS_4 (0 ≤ x ≤ 10) glass–ceramics. The conductivity increased with an increase of the x content from x=0 to 6 in the (100-x)Na_3PS_4•xNa_4SiS_4, whereas the activation energies were similar in the composition range. Improvement of the conductivities would be attributed to the increase of pre-exponential factor (σ_0). The 94Na_3PS_4•6Na_4SiS_4 glass–ceramic showed the highest conductivity of 7.4×10^{-4} S cm^{-1}, which was 1.7 times higher than the conductivity of the Na_3PS_4 glass–ceramic (x=0). The conductivity of glass-ceramics is affected by both precipitated crystalline phases and glass compositions. Although the conductivity of the Na_4SiS_4 glass (2×10^{-5} S cm^{-1} as shown in Fig. 5(a)) is higher than that of the Na_3PS_4 glass (6×10^{-6} S cm^{-1})[7], the conductivity of the 94 Na_3PS_4·6 Na_4SiS_4 glass–ceramic is two orders of magnitude higher than that of the Na_4SiS_4 glass. Thus, the contribution of glass composition to the conductivity enhancement of glass–ceramic (x=6) would be small. The origin of the conductivity enhancement is investigated by XRD measurement as shown in Fig. 3. Neither a clear shift of peak positions nor an increase in peak intensities of the cubic Na_3PS_4 was observed from partial substitution of Na_4SiS_4 for Na_3PS_4. To examine a possible formation of solid-solution, the Rietvelt analysis for the XRD data of the glass-ceramics is now in progress. In addition, detailed structural analyses of the glass–ceramics using neutron and/or synchrotron X-ray diffraction are necessary for further discussion.

The electrochemical window of the $90Na_3PS_4 \cdot 10Na_4SiS_4$ glass–ceramic electrolyte was examined using cyclic voltammetry. As depicted in Figure 6, cathodic and anodic currents that are respectively attributable to sodium deposition and dissolution were observed at about 0 V vs. Na^+/Na. No significant current attributable to electrolyte decomposition was detected up to 5 V vs. Na^+/Na. These results suggest that the Na_3PS_4-Na_4SiS_4 glass–ceramic electrolyte exhibited a wide electrochemical window of 5 V and that it was electrochemically stable against Na metal.

4. Conclusions

For this study, $(100-x)Na_3PS_4 \cdot xNa_4SiS_4$ milled samples were prepared using a planetary ball mill apparatus. The cubic Na_3PS_4 phase was crystallized directly in as-prepared samples at the composition range of $0 \leq x \leq 10$. Amorphous materials were obtained for samples between $25 \leq x \leq 100$. All as-prepared samples showed conductivities of about 10^{-5} S cm^{-1} at 25°C.

The $(100-x)Na_3PS_4 \cdot xNa_4SiS_4$ glass–ceramics were prepared by heat treatment of the milled samples. Unknown crystals were precipitated in glass–ceramics at the compositions of x=25, 67, and 100. The conductivities of the glass–ceramics were lower than those of the milled samples. In the composition range of $0 \leq x \leq 10$, the cubic Na_3PS_4 phase was only crystallized in the glass–ceramics. Their conductivities were greater than 10^{-4} S cm^{-1} at 25°C. Glass–ceramics with 6 mol% Na_4SiS_4 showed the highest conductivity of 7.4×10^{-4} S cm^{-1}, which is higher than that of Na_3PS_4 glass–ceramic without Na_4SiS_4. Cyclic voltammetry showed that the $90Na_3PS_4 \cdot 10Na_4SiS_4$ glass–ceramic electrolyte exhibited a wide electrochemical window of 5 V. The Na_3PS_4-Na_4SiS_4 glass–ceramic electrolytes showed not only high ionic conductivity but also high electrochemical stability. Therefore, this electrolyte system presents benefits for improving all-solid-state sodium secondary batteries.

Acknowledgements

This research was financially supported by JST, “Advanced Low Carbon Technology Research and Development Program (ALCA)”

References

[1] M. Armand and J. M. Tarascon, *Nature,* 2008, **451**, 652.

[2] J. M. Tarascon and M. Armand, *Nature,* 2001, **414**, 359.

[3] C. Delmas, J. Braconnier, C. Fouassier and P. Hagenmuller, *Solid State Ionics,* 1981, **3-4**, 165.

[4] S. Komaba, C. Takei, T. Nakayama, A. Ogata and N. Yabuuchi, *Electrochem. Commun.,* 2012, **12**, 355.

[5] M. Nishijima, I. D. Gocheva, S. Okada, T. Doi, J. I. Yamaki and T. Nishida, *J. Power Sources*. 2009, **190**, 558.

[6] C. W. Park, H. S. Ryu, K. W. Kim, J. H. Ahn, J. Y. Lee and H. J. Ahn, *J. Power Sources*, 2007, **165**, 450.

[7] A. Hayashi, K. Noi, A. Sakuda and M. Tatsumisago, *Nat. Commun.*, 2012, **3**, 856.

[8] A. Hayashi, K. Noi, N. Tanibata, M. Nagao and M. Tatsumisago, *J. Power Sources*, 2014, **258**, 420.

[9] R. Kanno and M. Maruyama, *J. Electrochem. Soc.*, 2001, **148**, A742.

[10] N. Kamaya, K. Homma, Y Yamakawa, M Hirayama, R Kanno, M Yonemura, T Kamiyama, Y Kato, S Hama, K Kawamoto and A Mitsui, *Nat. Mater.*, 2011, **10**, 682.

[11] A. Hayashi, Y. Ishikawa, S. Hama, T. Minami and M. Tatsumisago, Electrochem. *Solid-State Lett.*, 2003, **6**, A47.

Figure caption

Figure 1 XRD patterns of the (100-x)Na_3PS_4·xNa_4SiS_4 (mol%) mechanically milled samples. The numbers in brackets are milling period of time. Inverted triangle denotes the diffraction peaks attributable to the cubic Na_3PS_4 phase.[7]

Figure 2 DTA curves of the (100-x)Na_3PS_4·xNa_4SiS_4 mechanically milled samples.

Figure 3 XRD patterns of the (100-x)Na_3PS_4·xNa_4SiS_4 heat-treated (glass-ceramic) samples. A silicon powder as an internal standard was added to the glass-ceramic powders in the composition range of $0 \leq x \leq 5$.

Figure 4 Temperature dependence of the conductivities of the 94Na_3PS_4·6Na_4SiS_4 (mol%) glass-ceramic sample. Inset is a complex impedance plot of the glass-ceramic sample at room temperature.

Figure 5 (a) Composition dependence of the room temperature conductivities for the (100-x)Na_3PS_4·xNa_4SiS_4 samples. Open and closed circles denote the conductivities for the as-prepared samples and heat-treated (glass-ceramic) samples, respectively. (b) Composition dependence of the room temperature conductivities and the activation energies for conduction of the (100-x)Na_3PS_4·xNa_4SiS_4 ($0 \leq x \leq 10$) glass-ceramic samples. Circles and triangles denote the conductivities and the activation energies, respectively.

Figure 6 Cyclic voltammogram of the 90Na_3PS_4·10Na_4SiS_4 glass-ceramic sample.

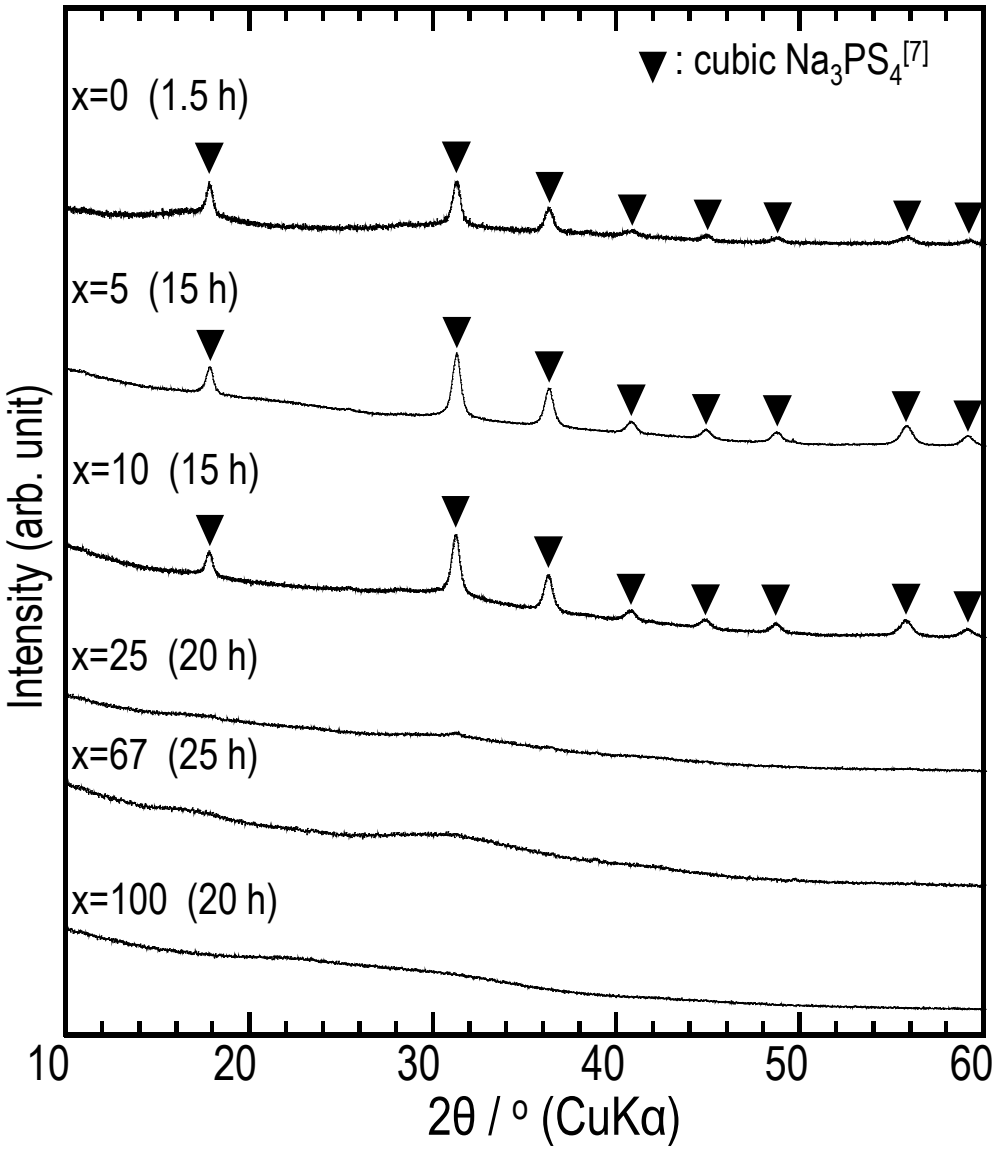

Fig. 1

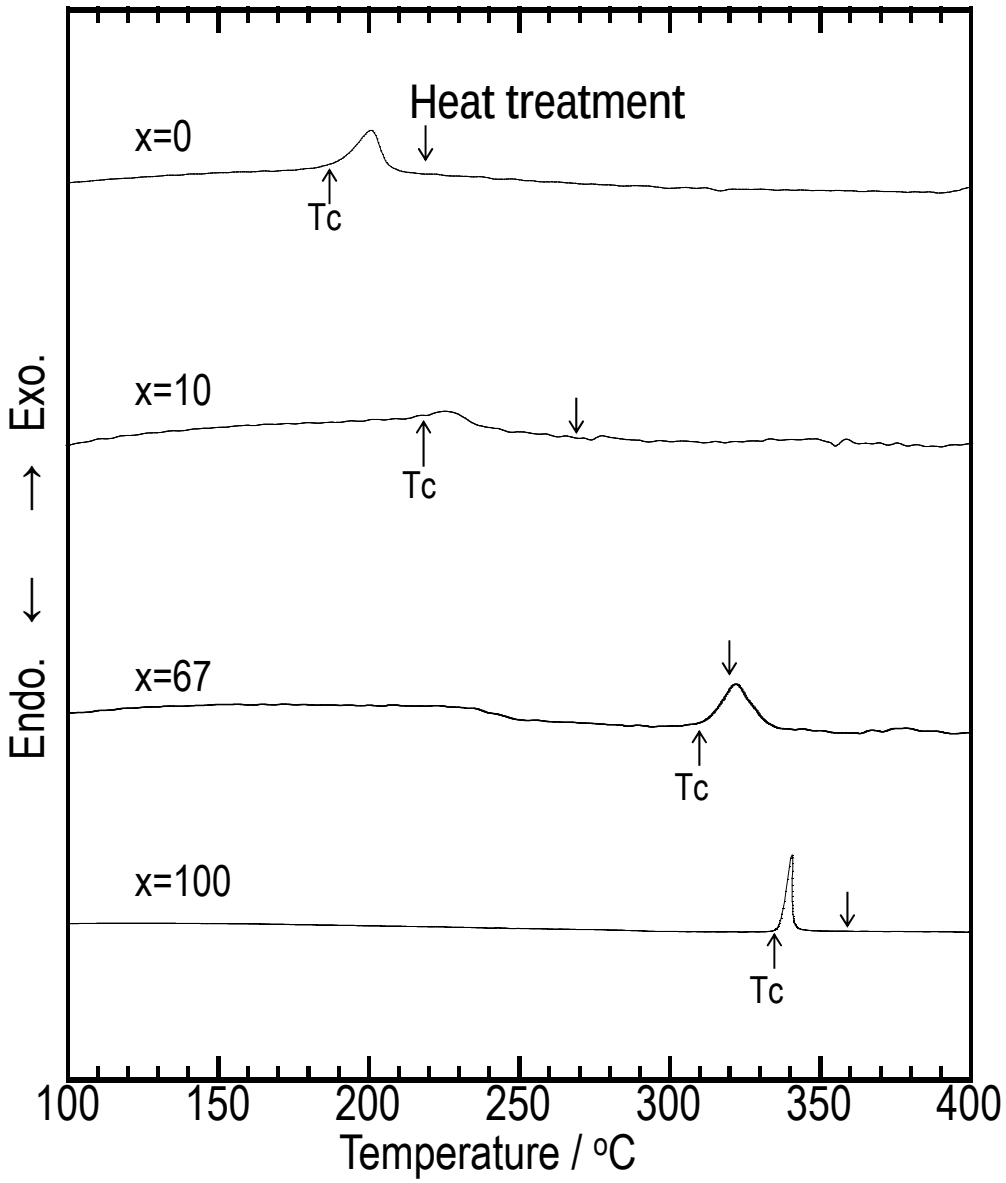

Fig. 2

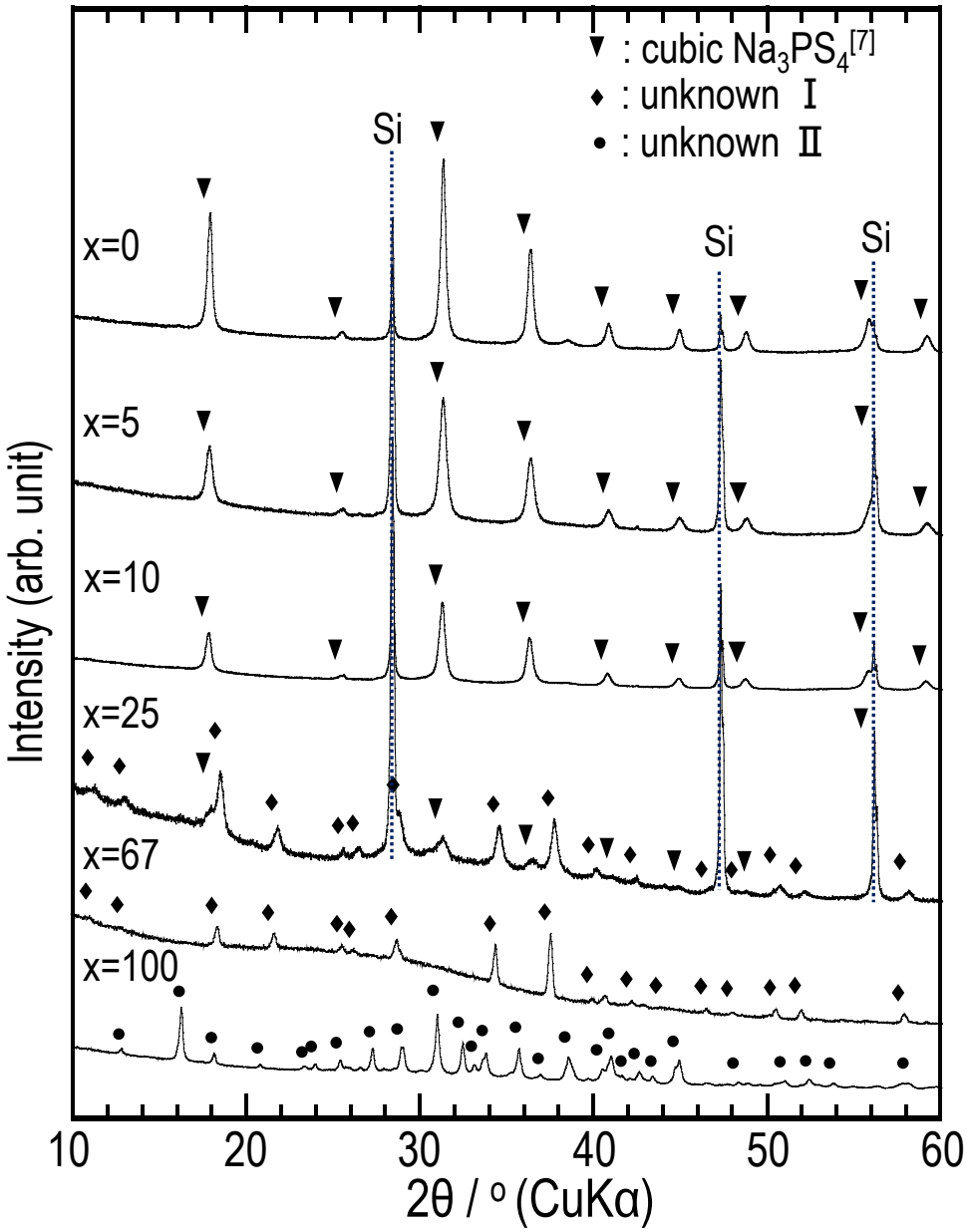

Fig. 3

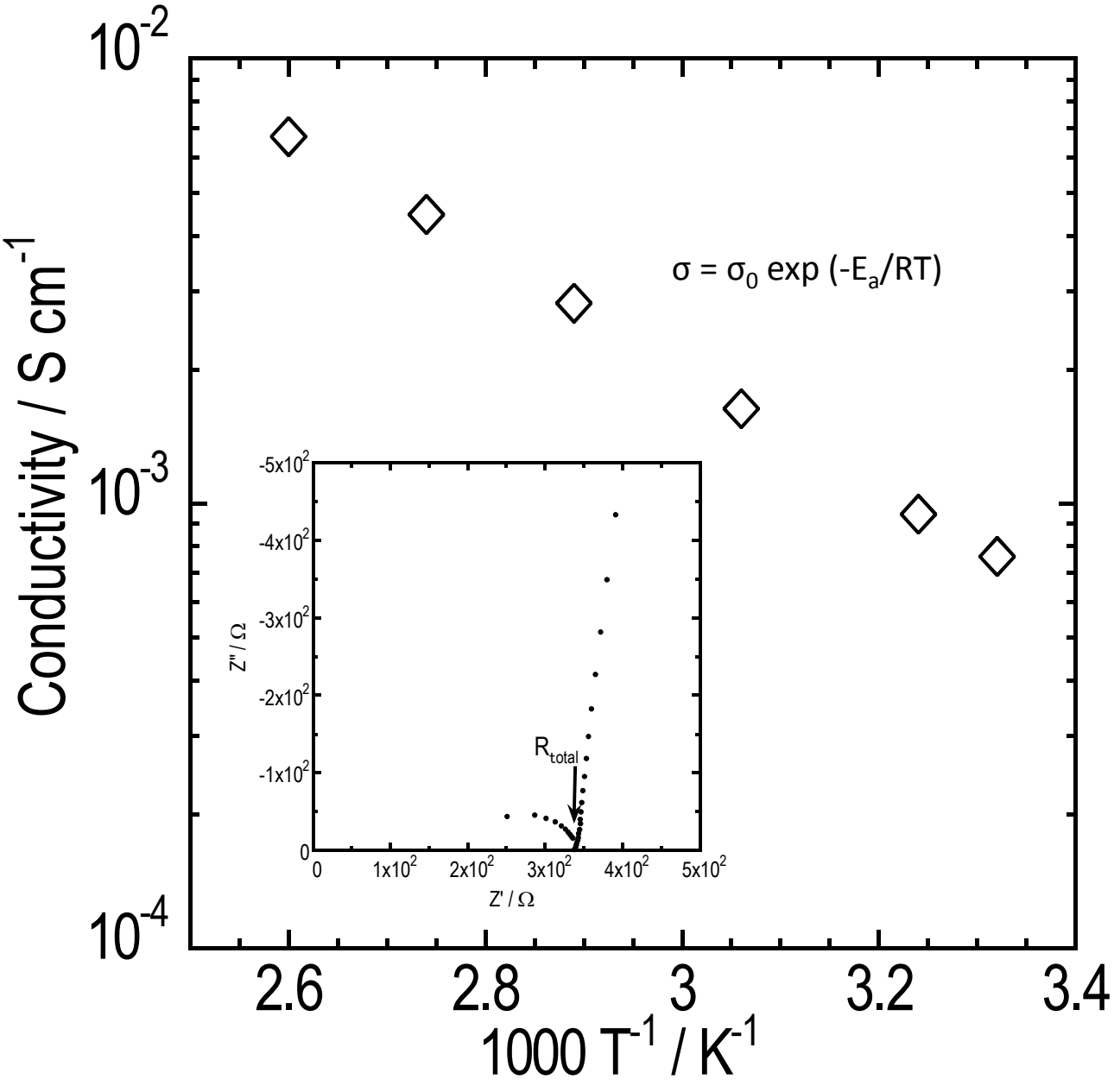

Fig. 4

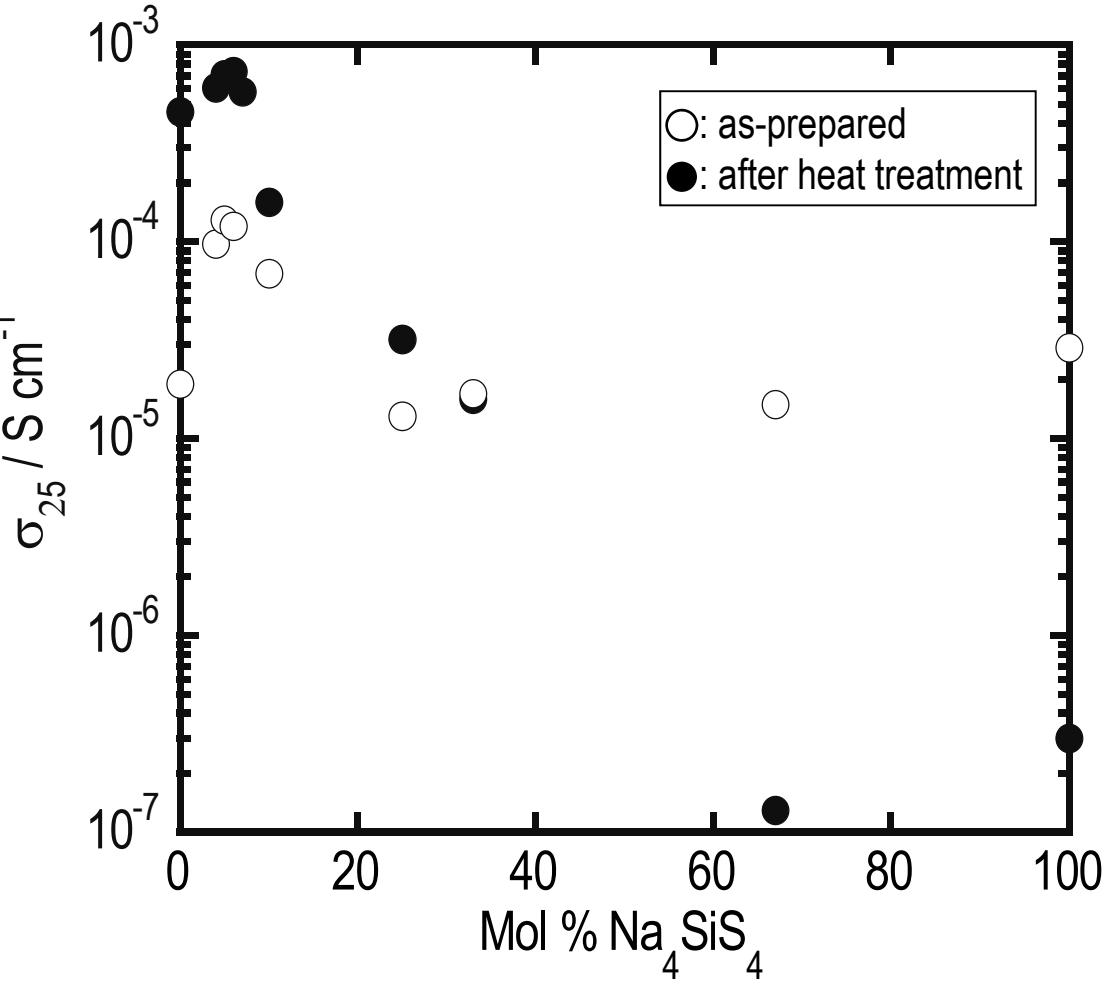

Fig. 5(a)

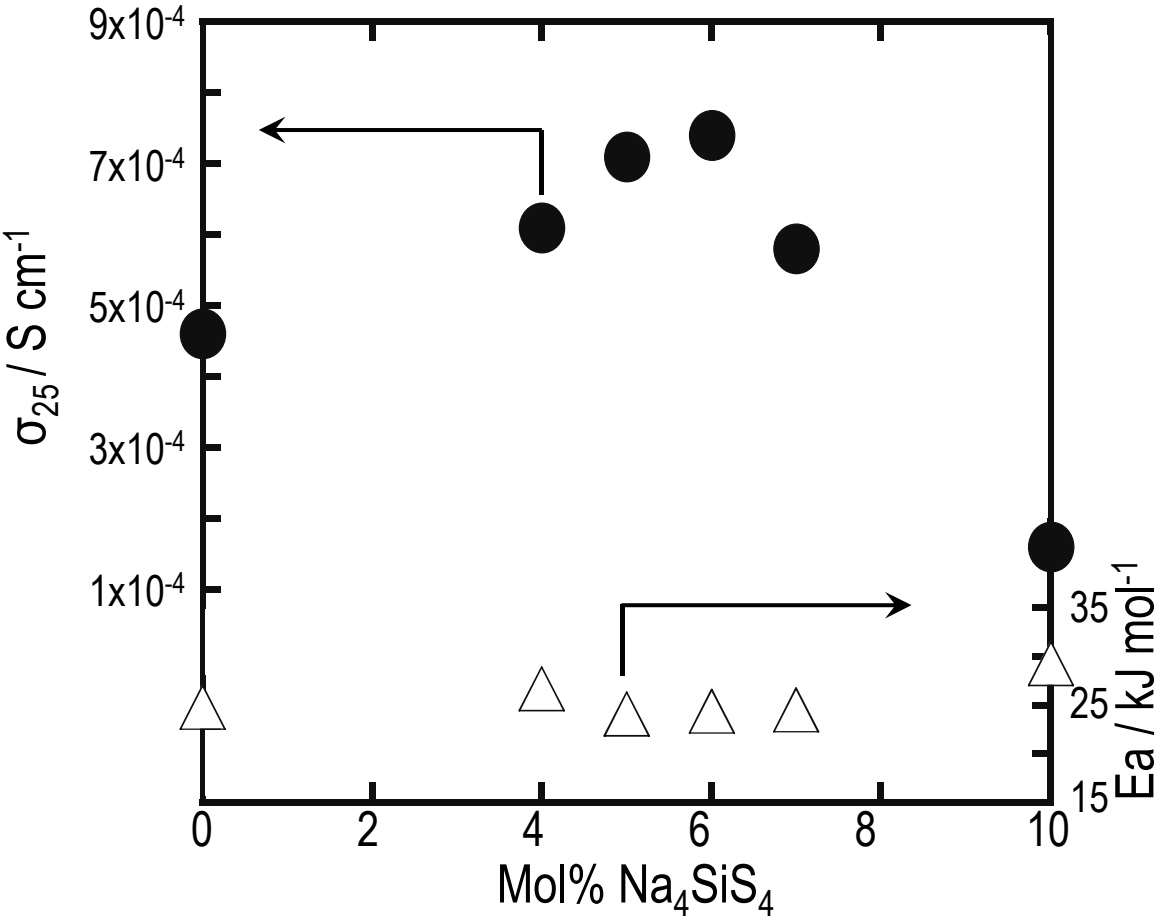

Fig. 5(b)

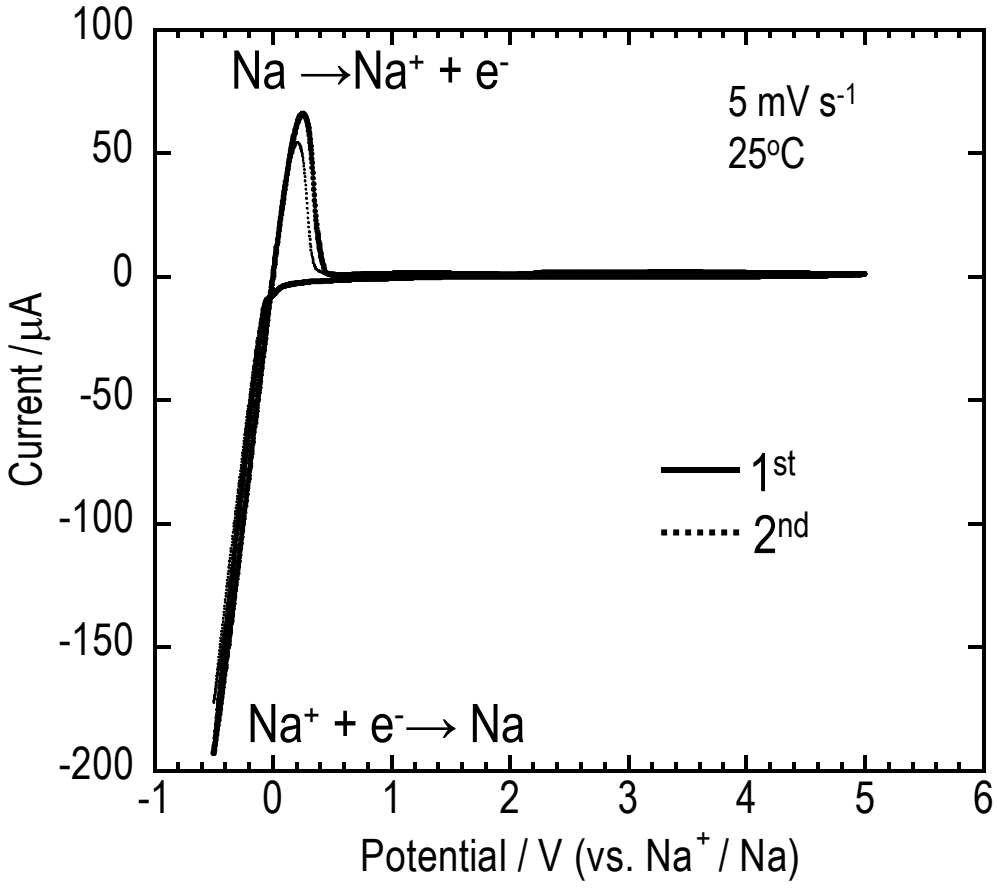

Fig. 6